Eur. Phys. J. Appl. Phys. (2017) 77: 20501
DOI: 10.1051/epjap/2017160410

THE EUROPEAN PHYSICAL JOURNAL APPLIED PHYSICS

Regular Article

Flexural vibration bandgaps in local resonance beam with a novel two-degree-of-freedom local resonance system

Kuan Lu, Jiu Hui Wu[a], Li Jing, and Dong Guan

School of Mechanical Engineering and State Key Laboratory for Strength and Vibration of Mechanical Structures, Xi'an Jiaotong University, 710049 Xi'an, P.R. China

Received: 3 November 2016 / Accepted: 3 February 2017

Abstract. In this paper, an elastic metamaterial beam with a novel two-degree-of-freedom local resonator is investigated theoretically, and the dispersion relation is calculated by using transfer matrix (TM). In order to confirm the existence of band gaps, the transmission spectrum of flexural wave are also studied by using finite element method. The formation mechanism of the flexural vibration bandgaps (FVBGs) are further analyzed by studying the displacement fields of the eigenmodes at the band-gap edges. At last, the evolution of the dispersion relations with the increasing of the distance from the one side rubber to the center of the local resonance mass are discussed in detail, and the effects of the outside diameter of the Cu ring and the equivalent stiffness k of the rubbers on the FVBGs are also investigated. Through the above analysis, we can draw the following conclusions, due to the unequal of the torques provided by the two rubbers, two different rotational vibrations of local resonance mass with two different local resonance frequencies are introduced in the local resonance system, thus the elastic metamaterial beam shows two FVBGs at low frequencies. The theoretical results are in good agreement with the numerical results. The magnitude of torques introduced in the local resonance system can obviously affect the locations of the FVBGs. With the asymmetry decreasing, the frequency region of the first FVBG moves to the higher value, while that of the second FVBG tends to the lower value, and when the two torques are equal, the two FVBGs coupled into one wider gap. For the elastic metamaterial beam with heavy resonance mass and weak rubbers is appropriate to obtain a lower band gap, and the total width of the FVBGs becomes wider. However, it does just the opposite under the condition of the case with light Cu ring and strong rubbers, but the total width of the band gaps also becomes wider. The propagation properties of the flexural wave in the designed local resonance beam can potentially be used to control and insulate vibration at low-frequency range and the unequal distances between the two rubbers to the center of the local resonance mass provide possibilities to expand the application of the beams for the vibration control in the needed frequency ranges.

1 Introduction

The propagation of elastic waves in periodic composite materials (phononic crystals, PCs) has been received a great deal of attention over the recent 20 years [1–8]. And due to the existence of bandgaps within the PCs, the propagation of acoustic/elastic waves are fully forbidden, which has potential applications in various fields, such as noise and vibration isolation, frequency filters, and so on.

The Bragg scattering and local resonance are the two kinds of formation mechanisms for the band gaps. The Bragg scattering bandgaps are caused by multiple scattering of the periodic inclusions, and the elastic wavelength of the band gap frequencies is of the same order to the structural period [1,2]. While the local resonance bandgaps are caused by the interaction between local resonance system and the elastic wave, and the frequency range of the local resonance band gaps is almost two orders of magnitude lower than that of the Bragg scattering [3–8], which makes this type of local resonance PCs more widely used in low-frequency vibration attenuation and sound insulation [9–27]. Among them, the propagation of the vibrations in PC beams has attracted a great deal of attention for several years due to the widespread applications of beam structures in engineering. Wang et al. [10] studied the dispersion relation of the infinite quasi-one-dimensional beams by using an improved lumped-mass method, and the low-frequency band gap was obtained, this provided a new way for the low-frequency vibration insulation. Wen et al. [11] reported a periodic binary straight beam with different cross sections, and the band structures of flexural waves were calculated

[a] e-mail: ejhwu@mail.xjtu.edu.cn

by using the plane-wave expansion method. Based on this, he also designed a vibration isolation structure with an attenuation of about 30 dB in the frequency region of the band gaps. Yu et al. [13] investigated the flexural vibration band gaps of the Timoshenko beams with periodic spring-mass system by using the transfer matrix method, and the vibration band gap is found at low frequencies. Subsequently, Wu and Hsu [14] studied the free vibration analysis of the simply supported beams carrying multiple point masses and spring-mass systems by using a new method, and the effect concerning mass of each helical spring was also presented. Yu et al. [15] analyzed the wave numbers and traveling wave characteristics in the periodic beam on elastic foundations, and he found that the wide flexural wave band gap existed at low frequencies. Through the above analysis, it can be found that those researches were based on the single-degree-of-freedom local resonance system. Recently, the multiple-degree-of-freedom local resonance system has been aroused great interest from researchers for good low-frequency broadband bandgaps [16–27]. Yu et al. [19] first reported the flexural vibration band gaps in Euler-Bernoulli beams with two-degree-of-freedom locally resonant structures, and the vertical and rotational vibration of a resonator was introduced in the calculation. Pai and Peng [22] presented a new metamaterial beam which consists of a uniform isotropic beam and small two mass-spring-mass local resonance subsystems, two stop-bands was demonstrated and the bandgaps mechanism were explained by the concept of negative effective mass and effective stiffness. However, the FVBGs were opened by the translation vibration of the local resonance mass in the existing literature, the rotational vibrations of the local resonance mass had not been considered, and its adjustment mechanism on the band gaps is also unclear.

In this paper, the band structures of a novel two-degree-of-freedom local resonance beam which introduces the rotational vibration of local resonance mass are investigated theoretically and numerically. In order to verify the existence of the band gaps, the transmission spectrum of flexural wave are also studied by using finite element method. The formation mechanism of the FVBGs are further analyzed by studying the displacement fields of the eigenmodes at the band-gap edges. At last, the evolution of the dispersion relations with the increasing of the distance from the one side rubber to the center of the resonance mass, and the effects of the outside diameter of the Cu ring and the equivalent stiffness k of the rubbers on the FVBGs are discussed in detail.

2 Theory of the TM

Figure 1a shows the spring-mass model of the local resonance beam with the two-degree-of-freedom resonators periodically attached on it. The local resonance mass m and the base beam is connected by two spring k, and the distance between the two attachment points to the gravity O_n are l_1 and l_2, respectively. The lattice constant is a.

The governing equation for the time-harmonic free flexural vibration of the Euler-Bernoulli beam can be written as:

$$\frac{\partial^2}{\partial x^2}\left[EI\frac{\partial^2 y\,(x,t)}{\partial x^2}\right]+\rho A\frac{\partial^2 y\,(x,t)}{\partial t^2}=0, \tag{1}$$

where ρ is the density, E is the Young's modulus, A is the cross section area, and I is the moment of inertia with respect to the axis perpendicular to the beam axis. $y(x,t)$ represents the dynamic displacement at x.

The form of solution for equation (1) can be expressed as:

$$y(x,t)=X(x)\exp(i\omega t), \tag{2}$$

where $X(x)$ is the vibration amplitude, ω is the circular frequency.

For an Euler-Bernoulli beam, $X(x)$ can be expressed as:

$$X(x)=A\cos(\lambda x)+B\sin(\lambda x)+C\cosh(\lambda x)+D\sinh(\lambda x), \tag{3}$$

where $\lambda^4=\rho A\omega^2/EI$ is the flexural wave number.

For the first section $n1$ of the unit cell as shown in Figure 1b, the vibration amplitude can be written as:

$$X_{n1}(x_1)=A_{n1}\cos(\lambda x_1)+B_{n1}\sin(\lambda x_1)+C_{n1}\cosh(\lambda x_1)+D_{n1}\sinh(\lambda x_1), \tag{4}$$

where $x_1=x-na$, $na\le x\le na+L$, $L=l_1+l_2$.

Similarly, the amplitude of the second section $n2$ can be written as:

$$X_{n2}(x_2)=A_{n2}\cos(\lambda x_2)+B_{n2}\sin(\lambda x_2)+C_{n2}\cosh(\lambda x_2)+D_{n2}\sinh(\lambda x_2), \tag{5}$$

where $x_2=x-na$, $na+L\le x\le(n+1)\,a$.

The force equilibrium of the local resonance mass m and the base beam are shown in Figures 1c and 1d, respectively. For the base beam, the forces along the y-axis are only considered, while for the local resonance mass m, the moment about the center of the gravity O_n is also considered. According to analysis of force equilibrium of the local resonator, one can obtain:

$$-f_{n1}(t)-f_{n2}(t)-m\ddot{z}_n(t)=0, \tag{6}$$

$$f_{n1}(t)l_1-J\ddot{\theta}(t)-f_{n2}(t)l_2=0, \tag{7}$$

where $f_{n1}(t)$ and $f_{n2}(t)$ are the interactive forces between the local resonance mass m and the base beam at the two attaching points x_{n1} and x_{n2}, respectively, m and J are the mass and the moment of inertia of the local resonance mass, respectively. $z_n(t)=V_n\exp(i\omega t)$ and $\theta_n(t)=\Theta_n\exp(i\omega t)$ are the translational and rotational displacement of the local resonator m, respectively, and V_n and Θ_n are the amplitude of displacement and the rotational angle, respectively.

The force $f_{n1}(t)$ and $f_{n2}(t)$ can be obtained as following:

$$\begin{aligned}f_{n1}(t)&=k\left[z_n(t)-y(x_{n1},t)-l_1\theta_n(t)\right]\\&=k\left[V_n-X_{n1}(x_{n1})-l_1\Theta_n\right]\exp(i\omega t)\\&=F_{n1}\exp(i\omega t),\end{aligned} \tag{8}$$

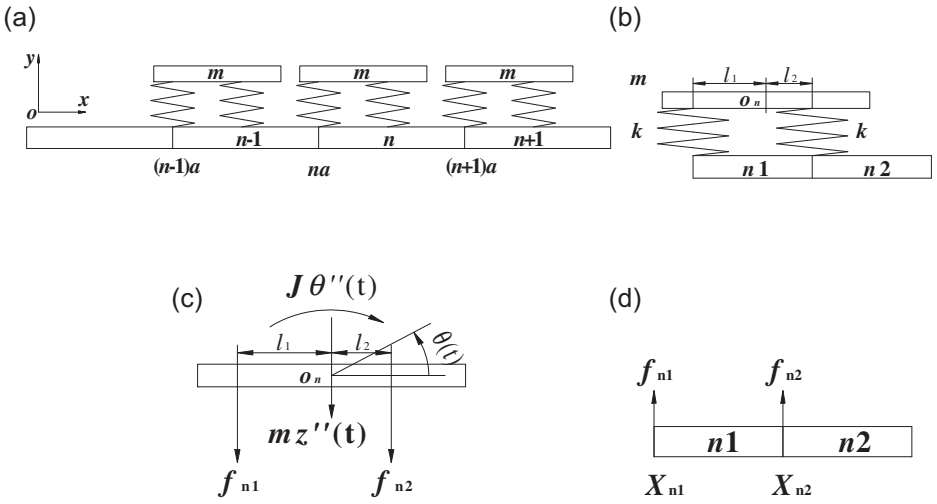

Fig. 1. Schematic diagram of (a) the novel two-degree-of-freedom local resonance beam, (b) the unit cell, the force equilibrium of (c) the local resonator m and (d) the base beam.

$$\begin{aligned} f_{n2}(t) &= k\left[z_n(t) - y(x_{n2},t) + l_2\theta_n(t)\right] \\ &= k\left[V_n - X_{n2}(x_{n2}) + l_2\Theta_n\right]\exp(i\omega t) \\ &= F_{n2}\exp(i\omega t). \end{aligned} \tag{9}$$

Substituting equations (8) and (9) into equations (6) and (7), leads to:

$$\left(2k - m\omega^2\right)V_n + k(l_2 - l_1)\Theta_n = k\left[X_{n1}(x_{n1}) + X_{n2}(x_{n2})\right], \tag{10}$$

$$\begin{aligned} k(l_1 - l_2)V_n &+ (J\omega^2 - kl_1^2 - kl_2^2)\Theta_n \\ &= k\left[X_{n1}(x_{n1})l_1 - X_{n2}(x_{n2})l_2\right]. \end{aligned} \tag{11}$$

Using equations (10) and (11), one can obtain:

$$V_n = MX_{n1}(x_{n1}) + NX_{n2}(x_{n2}), \tag{12}$$

$$\Theta_n = UX_{n1}(x_{n1}) + WX_{n2}(x_{n2}), \tag{13}$$

where

$$M = \frac{k\left(J\omega^2 - kl_2^2 - kl_1l_2\right)}{\left(2k - m\omega^2\right)\left(J\omega^2 - kl_1^2 - kl_2^2\right) + k^2\left(l_1 - l_2\right)^2},$$

$$N = \frac{k\left(J\omega^2 - kl_1^2 - kl_1l_2\right)}{\left(2k - m\omega^2\right)\left(J\omega^2 - kl_1^2 - kl_2^2\right) + k^2\left(l_1 - l_2\right)^2},$$

$$U = k\frac{\left(2k - m\omega^2\right)l_1 - k\left(l_1 - l_2\right)}{\left(2k - m\omega^2\right)\left(J\omega^2 - kl_1^2 - kl_2^2\right) + k^2\left(l_1 - l_2\right)^2},$$

$$W = -k\frac{\left(2k - m\omega^2\right)l_2 + k\left(l_1 - l_2\right)}{\left(2k - m\omega^2\right)\left(J\omega^2 - kl_1^2 - kl_2^2\right) + k^2\left(l_1 - l_2\right)^2}.$$

Using equations (4) and (5), one can obtain:

$$X_{n1}(x_{n1}) = X_{n1}(0) = A_{n1} + C_{n1}, \tag{14}$$

$$\begin{aligned} X_{n2}(x_{n2}) = X_{n2}(L) &= A_{n2}\cos(\lambda L) + B_{n2}\sin(\lambda L) \\ &+ C_{n2}\cosh(\lambda L) + D_{n2}\sinh(\lambda L). \end{aligned} \tag{15}$$

The analysis of the force equilibrium of the unit cell have been finished, and the above results will be used to deal with the band structures of the two-degree-of-freedom local resonance beam.

According to the continuities of displacement, rotation angle, bending moment and shear force at X_{n2}, the boundary conditions can be expressed as:

$$X_{n1}(L) = X_{n2}(L), \tag{16a}$$

$$X'_{n1}(L) = X'_{n2}(L), \tag{16b}$$

$$EIX''_{n1}(L) = EIX''_{n2}(L), \tag{16c}$$

$$EIX'''_{n1}(L) = EIX'''_{n2}(L) - F_{n2}. \tag{16d}$$

Substituting equations (4) and (5) into equations (16a)–(16d) and using equations (12) and (13), one can obtain the matrix form as following:

$$K_1\Psi_{n2} = H_1\Psi_{n1}, \tag{17}$$

where $\Psi_{n2} = \left[A_{n2}\ B_{n2}\ C_{n2}\ D_{n2}\right]^T$, $\Psi_{n1} = \left[A_{n1}\ B_{n1}\ C_{n1}\ D_{n1}\right]^T$.

Similarly, according to the continuities of displacement, rotation angle, bending moment and shear force at X_{n1}, the boundary conditions can be expressed as:

$$X_{(n-1)2}(a) = X_{n1}(0), \tag{18a}$$

$$X'_{(n-1)2}(a) = X'_{n1}(0), \tag{18b}$$

$$EIX''_{(n-1)2}(a) = EIX''_{n1}(0), \tag{18c}$$

$$EIX'''_{(n-1)2}(a) = EIX'''_{n1}(0) - F_{n1}. \tag{18d}$$

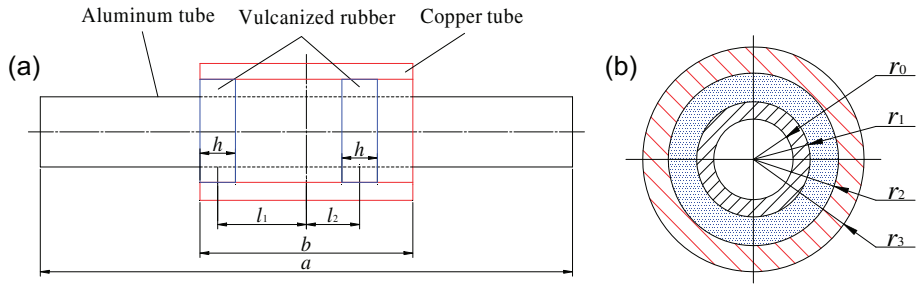

Fig. 2. Schematic diagrams of (a) the unit cell and (b) the cross section of the local resonance beam.

Analogously, we can obtain:

$$K_2\Psi_{n1} + K_3\Psi_{n2} = H_2\Psi_{(n-1)2}, \tag{19}$$

where $\Psi_{n2} = \left[\, A_{n2}\ B_{n2}\ C_{n2}\ D_{n2} \,\right]^T$,
$\Psi_{n1} = \left[\, A_{n1}\ B_{n1}\ C_{n1}\ D_{n1} \,\right]^T$,
$\Psi_{(n-1)2} = \left[\, A_{(n-1)2}\ B_{(n-1)2}\ C_{(n-1)2}\ D_{(n-1)2} \,\right]^T$.
Using equations (17) and (19), we can get the relation between the nth cell and the $(n-1)$th cell,

$$\Psi_{n2} = T\Psi_{(n-1)2}, \tag{20}$$

where $T = \left[K_2H^{-1}K_1 + K_3\right]^{-1} H_2$ is the transfer matrix.

Due to the periodicity of the infinite system along the x-axis, using the Bloch theorem we can obtain:

$$\Psi_{n2} = e^{ika}\Psi_{(n-1)2}, \tag{21}$$

where k is the wave vector in the x direction.

Using equations (20) and (21), we can obtain the standard eigenvalue problem of 4×4 matrix:

$$\left|T - e^{ika}I\right| = 0, \tag{22}$$

where I is the 4×4 unit matrix. By solving the eigenvalue of the matrix T, the dispersion relation between the wave vector k and the circular frequency ω can be obtained.

3 Results and discussion

3.1 Band structures and transmission spectrum

In this paper, the focus is to study the changes of dispersion relation caused by the rotation vibration of the local resonance system. Similar to the structure in reference [19], the beam with periodic local resonance structures is shown in Figure 2. The structural dimensions and the material parameters are basically the same as the model in reference [19]. The base beam and the local resonance mass are constructed from an aluminum tube and a copper tube, respectively, and the size for the structure are $r_0 = 7 \times 10^{-3}$ m, $r_1 = 1 \times 10^{-2}$ m, $r_2 = 1.5 \times 10^{-2}$ m, $r_3 = 1.95 \times 10^{-2}$ m, $b = 6 \times 10^{-2}$ m, respectively. The width of the rubber ring is $h = 1 \times 10^{-2}$ m, and $l_1 = 2.5 \times 10^{-2}$ m, $l_2 = 1.5 \times 10^{-2}$ m. The lattice constant is $a = 1.5 \times 10^{-1}$ m. The material parameters are given in Table 1. The equivalent stiffness of the rubber ring is $k = 1.65 \times 10^5$ N/m [19].

Figure 3a shows the band structures results (red line) calculated by the method deduced in this paper. It can be seen that there are three flexural bands exist in the frequency range from 0 Hz to 800 Hz, where two FVBGs (dark gray regions) are involved. The lowest FVBG is from 154 Hz to 167 Hz with the width of 23 Hz, which is between the first and the second band. The second FVBG is from 198 Hz to 410 Hz with the width of 212 Hz, which is between the second and the third band.

In order to verify the correctness of the calculation method, the band structures (black dot line in Fig. 3a) and the transmission spectrum (black square-dots line in Fig. 3b) are also calculated by using FEM. The locations of the two FVBGs (from 149.99 Hz to 166.87 Hz and from 189.06 Hz to 393.34 Hz) is in very good agreement with the band structures calculated by the method proposed in this paper, and the correctness of the method is verified. As shown in Figure 3b, two frequency ranges with an obviously attenuation (the gray regions) can be found in the transmission spectrum, and their locations correspond well with the band gaps in Figure 3a.

3.2 Eigenmodes analysis

As we all know, when the frequency of the incident elastic wave is close to the nature frequency of the internal spring-mass system, the corresponding local resonance will be activated, and the two mass move in reversed phase with a reaction force acting on the beam against the harmonic elastic wave excitation. The vibration of the beam will be reduced or even restrained because of the interaction between the local resonances and the traveling wave modes, and thus forming the band gaps within these frequencies regions. The local resonance beam with single resonator previously studied have only one FVBG at low frequencies, but the novel local resonance beam proposed in this paper has two obvious band gaps. In order to further reveal this phenomenon, the eigenmode shapes and displacement vector fields of the modes labelled in the Figure 3a are shown in Figure 4.

In each color map of the displacement vector fields, the magnitude is calculated by $\sqrt{\left(u_x^2 + u_y^2 + u_z^2\right)}$. For mode A,

Table 1. Material parameters used in calculations.

Material	Mass density (kg/m^3)	Young's modulus (N/m^2)	Poisson's ratio
Aluminum	2800	7.2e10	0.35
Rubber	1300	1.2e5	0.47
Copper	8950	16.46e10	0.33

the resonator rotates along a fixed axis while the base beam keeps still, and the vibration energy is well concentrated in the local resonance system. The vibration of the resonators is coupled to the flexural vibration of the beam, thus retraining the vibration of the beam, and the FVBG opened at this frequency. For mode B, the dynamic stability is obtained between the base beam and the Cu ring (the local resonance mass), the vibration of the base beam can spread freely at this frequency and the first FVBG closed. The vibration state of mode C (the start frequency of the second FVBG) is similar to that of the mode A, what the difference between them is that the rotation axis of rotational vibration is not the same. For mode D, the local resonance mass keeps still while the base beam vibrates with large amplitude, the Cu ring and the beam vibrate in a reverse phase, and the second FVBG closed.

In reference [19], the rotation vibration of the local resonance mass is introduced in the calculation, and because the same distance of the two rubbers to the center of the Cu ring, the two FVBGs coupled into one band gap. While in this paper, the distance of each rubber to the center of the local resonator is unequal,which leads to appear two different local resonance frequencies and thus forming two FVBGs.

3.3 Effect of the distance l_2 on the FVBGs

From above analysis, due to the unequal between the distance l_1 and l_2, two different rotational local resonance frequencies appear, thus generating two FVBGs. And the band gaps are very sensitive to these two parameters. In order to study the effects of the locations of the two rubbers on the band gaps, the evolutions of the dispersion curves with the distance l_2 from an asymmetric state ($l_1 \neq l_2$) to a symmetric state ($l_1 = l_2$) are investigated in this section, and the regulatory mechanisms are discussed in detail.

Figure 5 shows the comparing the dispersion relations of the local resonance beams. It can be seen that the band structures of the beam with different local resonance systems differ obviously from each other. The distance l_2 has a very important effect on the second dispersion curve which plays an important role for the separating and coupling of band gaps, and meanwhile increasing the distance l_2 increase the frequency of the first band line at wave vector 1. When the distance l_2 increase gradually form an asymmetric distribution to a symmetric distribution, the frequency range of first FVBG move to a high value,while location of the second band keeps unchanged. The total

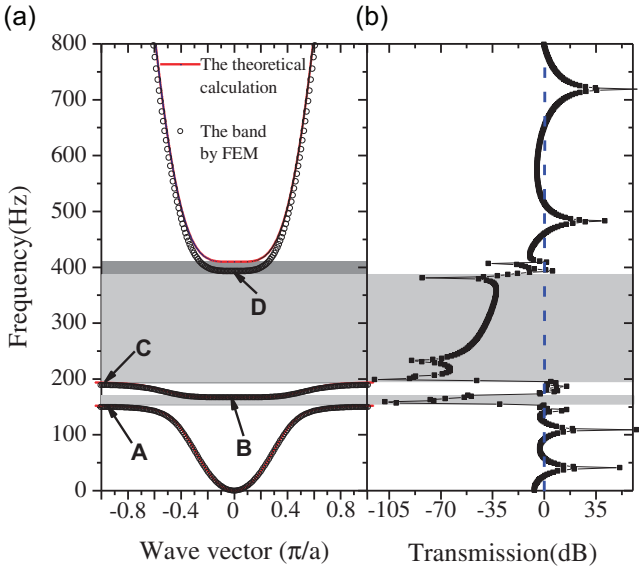

Fig. 3. The calculation results for (a) the band structures calculated by the transfer matrix method (the red line) and using FEM (black dot line) and (b) transmission spectrum of flexural vibration of the local resonance beam.

width of the band gaps almost keep the same. When in the case of $l_1 = l_2$, the two separate band gaps coupled into a wider band gap. It also can be found that the distance l_2 almost has no effect on the third band line.

In addition, it can also be found that as the distance l_2 increasing, the group velocity also changed obviously. The second band line approaching the horizontal exists in the model with distance l_1 being equal to the distance l_2, and this can be explained as zero wave velocity. From a technology perspective, the flat band may be used to generate frequency filter, and the wide FVBGs could be very useful in the vibration reduction of beam.

In order to further study the physical mechanism for the influence of distance l_2 on the band structures, the eigenmode shapes and displacement vector field of the modes labelled in Figure 5 are calculated by using FEM. For the modes A′, B′ and C′ are similar to modes A, B and C, the inequality between the two distances l_1 and l_2 causes the two different resonance frequencies of the local resonance system, thus generating two FVBGs. The only difference between the two cases is that, the resonance frequency of modes A′ and B′ are lower with lower first FVBG. For mode D′, the mode shape is very different from the lower band gap edge A′ and C′, the rotational vibration of local resonator is replaced by translational vibration due to the symmetric distribution of the two rubbers, and the vibration direction is vertical to the host beam. For modes E′ and F′, the vibration energy is also localized in the resonators, and they have the same vibration modes with the same resonance frequency. There is a dynamic balance within the local resonance system, and this kind of vibration mode is not coupled with the traveling wave in the beam, thus the FVBG does not open (Fig. 6).

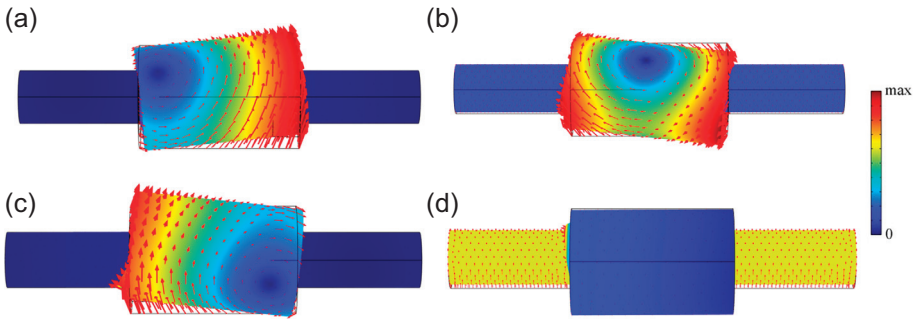

Fig. 4. Eigenmode shapes and displacement vector field of the modes labelled in Figure 3a.

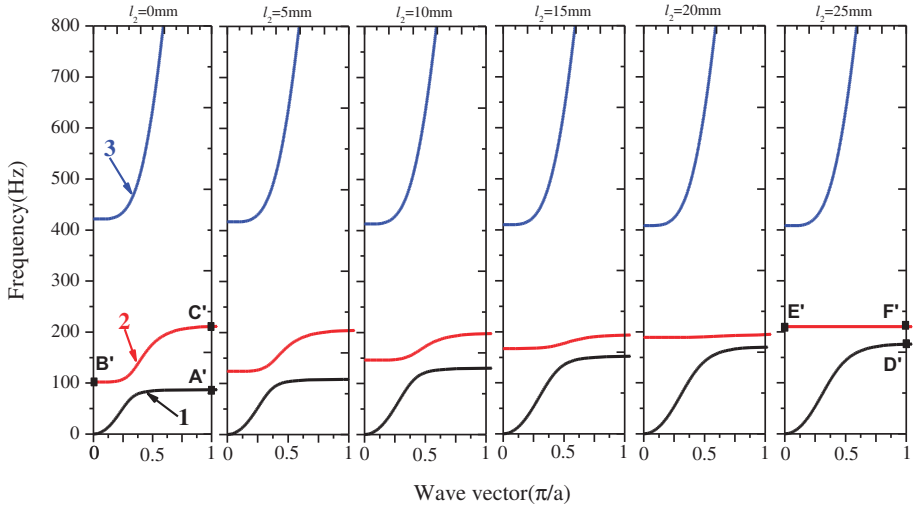

Fig. 5. Evolutions of the dispersion with the distance l_2 from an asymmetric distribution ($l_1 \neq l_2$) to a symmetric distribution ($l_1 = l_2$).

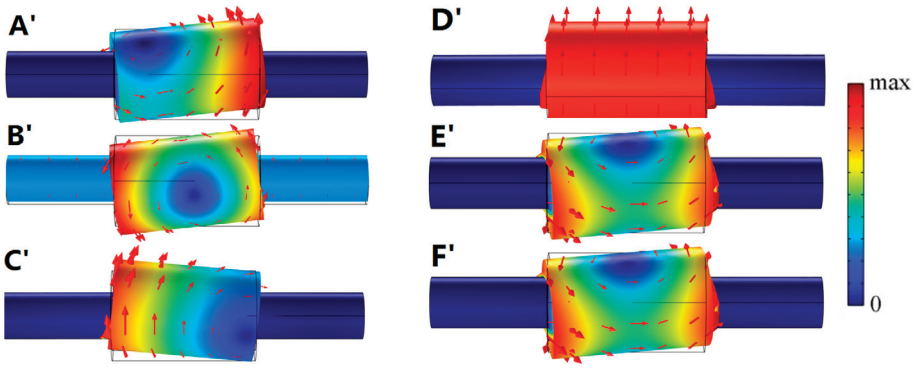

Fig. 6. Eigenmode shapes and displacement vector field of the modes labelled in Figure 5. A′–C′ and D′–F′ are the eigenmodes of the asymmetric and the symmetric local resonance beams, respectively.

3.4 Effect of the outside diameter r_3 on the FVBGs

Figure 7a shows the changes of the start frequency f_s, the cutoff frequency f_c, and the width of the FVBGs with the outside diameter r_3. It can be found that f_s and f_c of the first FVBG both decrease gradually with the increasing r_3, and the width of the first band gap has remained virtually unchanged. f_s and f_c of the second one both shift to a lower frequency when r_3 increased, but the decreasing rate of f_s is greater than that of f_c, which broadens the band gap.

With the increasing of the outside diameter r_3, the equivalent mass of the local resonator increases accordingly, and that will lead to the decrease of the local resonance frequencies, thus f_s and f_c of the two FVBGs both shift to a lower value. Meanwhile, the interactions between the local resonance and traveling wave modes are therefore increased, which broadens the total width of the FVBG.

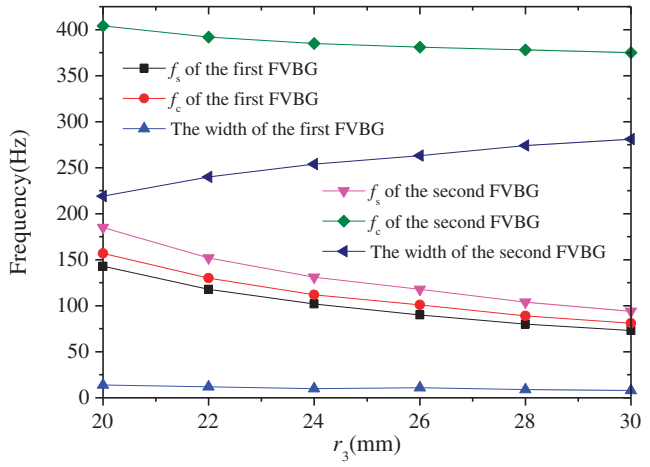

Fig. 7. The effect of the outside diameter of Cu ring r_3 on the FVBGs.

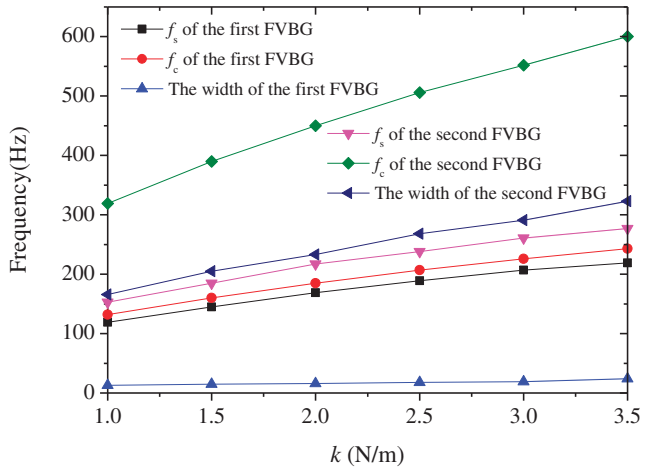

Fig. 8. The effect of the Equivalent stiffness of the rubbers k on the FVBGs.

3.5 Effect of the equivalent stiffness of the two rubbers k on the FVBGs

Figure 8 shows the equivalent stiffness of the two rubbers k on the FVBGs. It can be found that f_s and f_c of the first FVBG increase linearly with the increasing of the equivalent stiffness k, while the width of the band gap has little variation. However, f_s and f_c of the second FVBG as well as the bandwidth increase as the equivalent stiffness k increase. As mentioned above, the resonance mass rotates in the vertical direction with the base beam keeping still at the start frequencies of the FVBGs, and a rubber is stretched while the other is almost not deformed. When the equivalent stiffness is increased, the resonance frequencies are increased accordingly, which is also true for the upper boundaries of the band gaps. Moreover, the stronger rubbers enhance the interaction between the resonator and the vibration of the beam, that greatly broadens the width of the FVBGs.

4 Conclusions

In this paper, a new type two-degree-of-freedom local resonance beam is investigated theoretically, and the dispersion relations are calculated by using TM and FEM. In order to confirm the existence of band gaps, the transmission spectrum of flexural wave are also studied. The formation mechanism of the two FVBGs are further analyzed by studying the displacement fields of the eigenmodes at the bandgap edges. At last, the evolution of the dispersion relations with the increasing of the distance l_2,the effect of the outside diameter of the Cu ring and the equivalent stiffness of the rubbers on the FVBGs are in detail. Through the above analysis, we can draw the following conclusions, due to the unequal of the distance l_1 and l_2 for the designed local resonance beam, the rotational vibration of the local resonator is introduced in the local resonance systems, and two FVBGs are generated at low frequencies. The theoretical results are in good agreement with the numerical results. Meanwhile, the locations of the calculated transmission spectrum are in good agreement with the corresponding FVBGs regions. At the lower band-gap edges, the vibration is localized in the local resonance mass, while at upper band-gap edges, the local resonance mass and the base beam vibrate in a reverse phase. The two resonance frequencies are caused by the rotational vibration of the local resonance mass along the different rotation axis. Moreover, increasing the distance l_2 weakened the imbalance of the local resonator, and the two FVBGs coupled into a wider band gap. When the distance l_2 is reduced, the first FVBG shift to lower frequency regions while that of the second FVBG remain unchanged. For the elastic metamaterial beam with heavy resonance mass and weak rubbers is appropriate to obtain a lower band gap, and the total width of the FVBGs becomes wider. However, it does just the opposite under the condition of the case with light Cu ring and strong rubbers, but the total width of the band gaps also becomes wider. The propagation properties of the flexural wave in the designed local resonance beam can potentially be used to control and insulate vibration at low-frequency range.

The authors would like to thank the National Natural Science Foundation of China (Grant No. 51375362 and No. 51205305) for financial support.

References

1. M.S. Kushwaha, P. Halevi, L. Dobrzynski, B. Djafari-Rouhani, Phys. Rev. Lett. **71**, 2022 (1993)
2. R. Martínez-Sala, J. Sancho, J.V. Sánchez, V. Gómez, J. Llinares, F. Meseguer, Nature **378**, 241 (2002)
3. Z. Liu, X. Zhang, Y. Mao, Y. Zhu, Z. Yang, C. Chan, P. Sheng, Science **289**, 1734 (2000)
4. Z. Liu, C.T. Chan, P. Sheng, Phys. Rev. B **65**, 165116 (2002)
5. G. Wang, D. Yu, J. Wen, Y. Liu, X. Wen, Phys. Lett. A **327**, 512 (2004)

6. G. Wang, X. Wen, J. Wen, L. Shao, Y. Liu, Phys. Rev. Lett. **93**, 154302 (2004)
7. J.C. Hsu, T.T. Wu, Appl. Phys. Lett. **90**, 201904 (2007)
8. S. Naguleswaran, Int. J. Mech. Sci. **44**, 2463 (2002)
9. A. Khelif, B. Aoubiza, S. Mohammadi, A. Adibi, V. Laude, Phys. Rev. E **74**, 159 (2006)
10. G. Wang, J. Wen, X. Wen, Phys. Rev. B **71**, 104302 (2005)
11. J. Wen, G. Wang, D. Yu, H. Zhao, Y. Liu, J. Appl. Phys. **97**, 114907 (2005)
12. D. Zhou, T. Ji, Int. J. Solids Struct. **43**, 5555 (2006)
13. D. Yu, Y. Liu, G. Wang, H. Zhao, J. Qiu, J. Appl. Phys. **100**, 124901 (2006)
14. J.-S. Wu, T.-F. Hsu, Int. J. Mech. Sci. **49**, 834 (2007)
15. D. Yu, J. Wen, H. Shen, Y. Xiao, X. Wen, Phys. Lett. A **376**, 626 (2012)
16. L. Liu, M.I. Hussein, J. Appl. Mech. **79**, 011003 (2012)
17. Y. Xiao, J. Wen, D. Yu, X. Wen, J. Sound Vib. **332**, 867 (2013)
18. L. Raghavan, A.S. Phani, J. Acoust. Soc. Am. **134**, 1950 (2013)
19. D. Yu, Y. Liu, H. Zhao, G. Wang, J. Qiu, Phys. Rev. B **73**, 064301 (2006)
20. H. Huang, C. Sun, G. Huang, Int. J. Eng. Sci. **47**, 610 (2009)
21. K.T. Tan, H. Huang, C. Sun, Appl. Phys. Lett. **101**, 241902 (2012)
22. P.F. Pai, H. Peng, in *SPIE Smart Structures and Materials + Nondestructive Evaluation and Health Monitoring* (International Society for Optics and Photonics, Washington, 2014), pp. 90641X-90641X-21
23. Y. Liu, X. Su, C. Sun, J. Mech. Phys. Solids **74**, 158 (2015)
24. H. Peng, P.F. Pai, in *SPIE Smart Structures and Materials + Nondestructive Evaluation and Health Monitoring* (International Society for Optics and Photonics, Washington, 2015), pp. 94380X-94380X-19
25. W. Qian, Z. Yu, X. Wang, Y. Lai, B.B. Yellen, J. Appl. Phys. **119**, 055102 (2016)
26. H.J. Zhao, H.W. Guo, M.X. Gao, R.Q. Liu, Z.Q. Deng, J. Appl. Phys. **119**, 377 (2016)
27. X. Zhou, J. Wang, R. Wang, J. Lin, Appl. Phys. A **122**, 1 (2016)